MOLECULAR IMAGING AND BIOLOGY

Mol Imaging Biol (2019) 21:1064–1070
DOI: 10.1007/s11307-019-01352-3

Published Online: 15 April 2019

WMIS World Molecular Imaging Society
esmi European Society for Molecular Imaging

Check for updates

RESEARCH ARTICLE

Retrospective Brain Motion Correction in Glutamate Chemical Exchange Saturation Transfer (GluCEST) MRI

Dong-Hoon Lee,[1] Do-Wan Lee,[2] Jae-Im Kwon,[3] Chul-Woong Woo,[3] Sang-Tae Kim,[3] Jeong Kon Kim,[4] Kyung Won Kim,[4] Dong-Cheol Woo[3,5]

[1]*Faculty of Health Sciences and Brain and Mind Centre, The University of Sydney, Sydney, New South Wales, Australia*
[2]*Center for Bioimaging of New Drug Development, Asan Medical Center, Asan Institute for Life Sciences, Seoul, Republic of Korea*
[3]*MR Core Laboratory, Convergence Medicine Research Center, Asan Medical Center, Asan Institute for Life Sciences, Seoul, Republic of Korea*
[4]*Department of Radiology, Asan Medical Center, University of Ulsan College of Medicine, Seoul, Republic of Korea*
[5]*Department of Convergence Medicine, Asan Medical Center, University of Ulsan College of Medicine, Seoul, Republic of Korea*

Abstract

Purpose: To evaluate the feasibility of motion correction in glutamate chemical exchange saturation transfer (GluCEST) imaging, using a rat model of epileptic seizure.

Procedures: Epileptic seizure was induced in six male Wistar rats by intraperitoneal injection of kainic acid (KA). CEST data were obtained using a 7.0 T Bruker MRI scanner before and 3 h after KA injection. Retrospective motion correction was performed in CEST images using a gradient-based motion correction (GradMC) algorithm. GluCEST signals in the hippocampal regions were quantitatively evaluated with and without motion correction.

Results: Calculated GluCEST signals differed significantly between the pre-KA injection group, regardless of motion-correction implementation, and the post-KA injection group with motion correction (3.662 ± 1.393 % / 3.726 ± 1.982 % for pre-KA injection group with/without motion correction *vs.* 6.996 ± 1.684 % for post-KA injection group with motion correction; all $P < 0.05$).

Conclusions: Our results clearly show that GradMC can be used in CEST imaging for efficient correction of seizure-like motion. The GradMC can be further implemented in various CEST imaging techniques to increase the accuracy of analysis.

Keywords: Chemical exchange saturation transfer, Gradient-based motion correction, Glutamate, Retrospective motion correction

Introduction

Movement of the subject during magnetic resonance imaging (MRI) causes quality degradation of the image and misreading in quantitative evaluations [1–3]. The most fundamental reasons for motion effects occurrences in MR images are the long scan times that are required for high-resolution imaging. Degraded image quality not only causes a change in the anatomical structure but can also have a detrimental impact at the molecular level in quantification analyses. Therefore, performing motion correction prior to image analysis is an important consideration. To date, in order to solve the problems arising from motion effects, numerous studies have been performed using various prospective correction methods during the image acquisition process, as well as retrospective corrections that are performed after image acquisition [1, 4–6]. In addition, the autofocusing (AF) method has been

Dong-Hoon Lee and Do-Wan Lee contributed equally to this work.

Correspondence to: Dong-Cheol Woo; *e-mail:* dcwoo@amc.seoul.kr

introduced as a type of retrospective motion correction that does not require specialized data trajectory strategies, in contrast to prospective methods; however, this method requires reference data from navigator-based trackers in order to cope with a large number of unknown motion parameters [7–9]. Recently, gradient-based motion correction (GradMC), which is a modified form of the AF method, using small random initialization as the initial value for motion trajectory as well as motion trajectory gradient entropy metrics as a cost function, has also been introduced for advanced motion correction [10, 11]. This method iteratively corrects translation and rotation, until image quality can be improved no further.

Chemical exchange saturation transfer (CEST) MRI has been used for molecular level exploration *in vivo* and to detect metabolite content indirectly, based on exchange-related properties [12–14]. In particular, glutamate-CEST (GluCEST) imaging has been shown to be capable of imaging parenchymal glutamate levels in the brain by measuring the exchange of glutamate amine protons with bulk water [15]. GluCEST has been used in investigations in various clinical fields, such as epilepsy, neurodegeneration, schizophrenia, and Huntington's disease, for determining the glutamate distribution in the disease region of the brain [16–18]. Therefore, the CEST technique, including GluCEST, can be a powerful tool in clinical diagnosis, research, and in the pre-clinical field. However, its main disadvantage is that it requires a relatively long scan time to collect whole-voxel datasets and z-spectrum, while varying the resonance frequency around the water, which causes subject motion during scanning, resulting in image degradation.

In this study, we applied the GradMC algorithm to CEST data to investigate the feasibility of motion correction and to determine how the motion correction procedure affects qualitative and quantitative results in CEST imaging. Motion-corrupted CEST data, obtained using a rat model of epilepsy, were used to reflect arbitrary head motion inside the head coil due to seizure, and data analyses were performed with and without the motion correction algorithm before as well as after epileptic seizure.

Materials and Methods

CEST Experiments

All animal experiments were approved by the University of Ulsan Animal Care and Use Committee, and the experiments were performed in strict accordance with the recommendations in the Guide for the Care and Use of Laboratory Animals of the National Institutes of Health.

For epileptic seizure rat modeling, male Wistar rats ($n = 6$, 250–300 g, Orient Bio Inc., Seongnam, Rep. of Korea) were injected intraperitoneally with kainic acid (KA) [19, 20]. All rats were scanned at two time-points: before and 3 h after KA injection. We performed the first scan (pre-injection) after insertion of the intraperitoneal injection line for KA administration with the rat located outside the bore of the MRI system. The second scan (after injection) was performed after a manual injection to minimize the possible position changes during each scan session. All rats therefore remained anesthetized, with 1.5–2.0 % isoflurane in the air, for the total preparation and scanning period (approximately 240 min; 60 min for MR scanning and 180 min for delay after KA injection). The respiration of each rat was monitored online using a small-animal respiratory-gating system (SA Instruments Inc., Stony Brook, NY, USA), and its temperature was maintained at approximately 37.5 ± 0.5 °C using a warm-water circulating flat-bed (CW-05G Heated Circulating Water Bath; MIDSCI, St. Louis, USA) positioned around its body.

Images were acquired using a 7.0 T Bruker pre-clinical MRI scanner (PharmaScan 70/16, Brucker BioSpin GmbH, Germany). We performed local shimming using a region-of-interest (ROI, $34 \times 34 \times 34$ mm^3) covering the whole brain area, prior to imaging, to achieve a homogeneous magnetic field and a high signal-to-noise ratio in the MRI system. CEST data were acquired from +3.67 ppm to −3.67 ppm, in 0.33 ppm steps, using the turbo-RARE pulse sequence on a single slice. Each slice contains a well-observed hippocampus region, which is a well-known brain region to evaluate glutamate level changes in epilepsy [18, 21, 22]. The following parameters were implemented: repetition time/echo time = 4200 ms/36.4 ms, field of view = 30×30 mm^2, matrix size = 96×96, slice thickness = 1 mm, echo spacing = 6.1 ms, and RARE factor = 16). A long continuous-wave radiofrequency pulse (power = 5.6 μT, and saturation time = 1 s) was used for CEST saturation. For each CEST acquisition, B_0 map, using the double echo-time (1.9 and 2.6 ms) method, and B_1 map, using the double flip-angles (30° and 60°) method, scans were also acquired to correct field inhomogeneities in the CEST data [15, 23].

Motion Correction and Data Analysis

The GradMC algorithm, which uses the image gradient entropy metric, was applied to the CEST data, and it was constructed using the following equations: $\varnothing(u) = \mathcal{H}(D_x u) + \mathcal{H}(D_y u)$, $\mathcal{H}(u) = -v^{\top} \ln v$, $v = \sqrt{[(u \odot \bar{u})/(u^H u)]} \in \mathbb{R}_+^N$, $u \in \mathbb{C}^N$, where D_x and D_y finite difference matrices at x- and y-directions, $\mathcal{H}(\cdot)$ is a pixel entropy, u is an unknown image matrix with size of $n_x \cdot n_y$, and mathematical operators $\bar{}$ and $\odot$ indicate the complex conjugate and Hadamard product, respectively. Since the rigid-motion transformation matrix (A_θ) can be applied to a motion-corrupted image matrix y with the empirical inversion, the equation can also be defined as follows: $u_\theta = F^H A_\theta y$, where u_θ is the resulting image in the spatial domain, and F is an orthonormal Fourier matrix. Recovered motion parameters are regularized with a quadratic penalty on the differences of consecutive motion

parameters as follows: $\theta = \arg\min_{\theta\in\Theta} \phi\left(F^H A_\theta y\right) + \lambda \|D\theta\|^2$, where $D \in \{0, \pm 1\}^{6\cdot T\times 6\cdot T}$ is a finite difference matrix temporally ordered by phase encodes, T indicates the number of k-space lines, and $\lambda \in \mathbb{R}_+$ is a regularization parameter for smoothness (0.2 was used in this study). The translation correction corresponds to the multiplication of each k-space line combined with a linear phase ramp as follows: $\exp^{(-2\pi i k_x \theta_t)}$, where k_x is the Fourier coefficient of the affected view, and θ_t is a translation function in the spatial domain. The rotation correction was performed based on a deformed grid, which is determined by rotating the points of each k-space line with by time angles, and interpolation process to predict the values of the rotated point. Additionally, we performed a minimizing cost function using a multi-scale coarse-to-fine approach because the cost function used in this study was highly nonlinear considering logarithms and piecewise interpolation polynomials. Multi-scale coarse-to-fine approach refines the estimated motion parameters step-by-step from coarse to fine scales. Since the central region of the k-space contains lower frequency (high signal intensity), motion produces little offsets in the spatial domain. For this reason, it is easier to estimate and correct the motion in the coarsely sampled image. Therefore, GradMC performs the first iteration to find only the segments in the central region of the k-space surrounded by the unknown motion parameter gaps in the high-frequency views in the motion trajectory, and as the iteration progresses, the gaps reduced until the entire trajectory is recovered. More details of GradMC have been reported elsewhere [10]. We performed motion correction on the CEST data corresponding to each frequency offset, and then applied B_0 and B_1 corrections. For B_0 correction, motion-corrected CEST data were interpolated using a cubic spline, and each voxel value of ± 3.0 ppm image was replaced by the neighborhood CEST data value, according to the amount of shift in the frequency as calculated from the B_0 map. Finally, GluCEST contrasts were corrected using relative B_1 values that were calculated based on the B_1 map, to correct the B_1 field inhomogeneity [15]. To quantify CEST data, based on the ROI drawn manually in the hippocampus region, magnetization transfer ratio asymmetry (MTR_{asym}) curves from 0 ppm to 3.67 ppm were calculated using the following equation: $MTR_{asym}(\Delta\omega) = [S_{sat}(-\Delta\omega) - S_{sat}(+\Delta\omega)]/S_{sat}(-\Delta\omega)$, where $\pm\Delta\omega$ are symmetrically located downfield and upfield from the water frequency offset (0 ppm). The GluCEST signal was normalized with $Ssat(-\Delta\omega)$, which can increase the dynamic range of the CEST contrast [24]. The quantitative GluCEST signal was evaluated at 3.0 ppm in the MTRasym curve, and we implemented the GluCEST map using the GluCEST values computed pixel-by-pixel from the image. Data acquisition and analysis procedures are in Fig. 1. All image processing and motion correction procedures were performed using in-house written MATLAB R2014a (MathWorks, Inc., Natick, MA, USA) scripts.

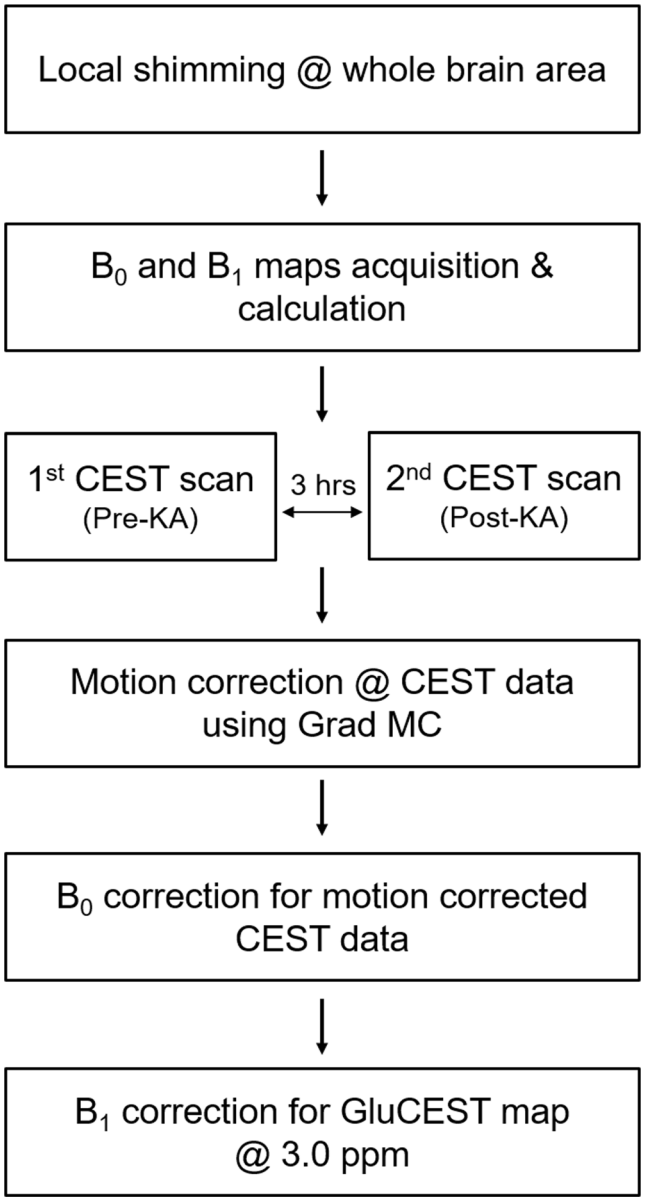

Fig. 1. Flow chart of CEST data acquisition, motion correction and analysis. CEST imaging scans were performed for two-time points: pre-KA and 3 h after KA injection. Then, retrospective motion correction was performed in frequency offsets for each CEST data. The B_0 field inhomogeneities calculated from field mapping were corrected in the motion-corrected CEST data. The relative B_1 map was used to correct the contrast in the glutamate CEST map. All CEST analysis procedures were performed on a voxel-by-voxel basis.

Statistical Analysis

For statistical analysis, the Wilcoxon rank-sum test was used to compare between the GluCEST signals that were motion corrected in the post-KA group and those signals in the pre-KA group, regardless of the motion correction. Moreover, this test was also used to compare between GluCEST signals

with and without motion correction in each group. A P value less than 0.05 was considered significant for all statistical analyses. All statistical analyses were performed using PASW statistics (version 18.0, SPSS Inc., Chicago, IL, USA).

Results

Figure 2 shows the MTR_{asym} curves in pre- and post-KA injection groups, with and without motion correction. The MTR_{asym} curves showed no significant differences in the pre-KA injection group (motion-free; Fig. 2a), regardless of motion correction. The MTR_{asym} curves in the post-KA injection group (motion-corrupted; Fig. 2b) showed clear differences after the application of motion correction. Notably, after correcting for the seizure-like motion in Fig. 2b, the MTR_{asym} curves were improved, with clearly reduced signal changes and standard errors.

Figure 3 shows the GluCEST signals in all groups calculated at 3.0 ppm. The GluCEST signals in each paired group was not significantly different (pre-KA injection group, with and without correction; 3.662 ± 1.393 % and 3.726 ± 1.982 %, respectively; $P = 0.773$, and post-KA injection group, with and without correction; 6.996 ± 1.684 % and 8.884 ± 6.401 %, respectively; $P = 0.989$). Since the pre-KA injection group had no motion, it is plausible that there were rarely GluCEST signal changes, irrespective of whether motion correction was applied. In addition, the post-KA injection group did not differ significantly after motion correction due to large range of standard error among the subjects without motion correction. Notably, as we expected, there were clear significant differences when we compared the results of the pre-KA injection group, regardless of motion correction, with those of the post-KA injection group with motion correction (3.726 ± 1.982 % *vs.* 6.996 ± 1.684 %; $P = 0.043$; without motion correction in the pre-KA injection group, and 3.662

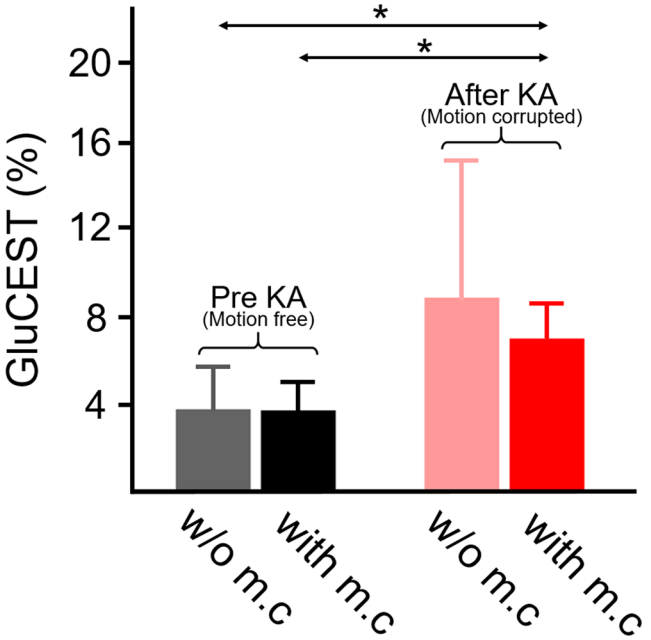

Fig. 3. Quantitative values of GluCEST signal for pre-KA (motion-free) and post-KA (motion-corrupted) injection with and without motion correction. (gray and pink bar plots: without motion correction, and black and red bar plots: with motion correction; $^*P < 0.05$).

± 1.393 % *vs.* 6.996 ± 1.684 %; $P = 0.037$; with motion correction in the pre-KA injection group).

Figure 4 shows the reconstructed GluCEST maps (pre-KA injection group without motion correction, Fig. 4a, and with correction Fig. 4b; post-KA injection group without motion correction Fig. 4c, and with correction Fig. 4d) from a representative rat. In the pre-KA injection group (Fig. 4a, b), there were rarely signal variations, regardless of motion correction, as indicated in Fig. 3. In contrast, in the post-KA injection group, distinctive seizure motion was markedly reduced by motion correction (Fig. 4c, d). Before

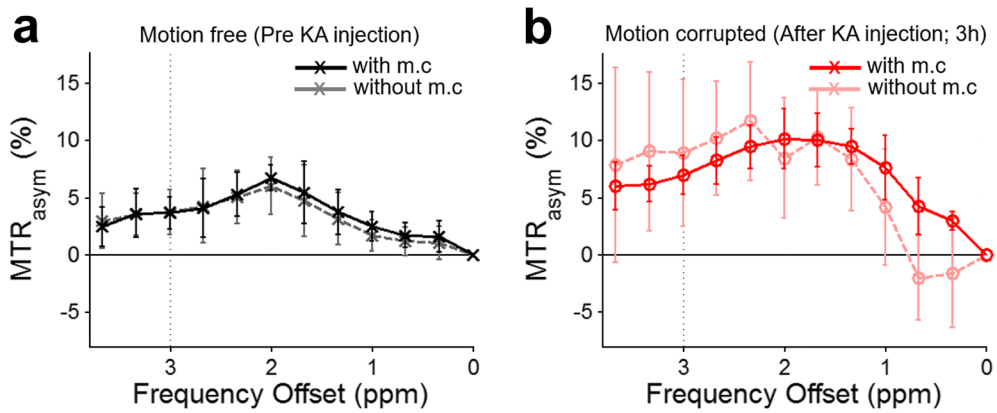

Fig. 2. Conventional MTR_{asym} curves **a** before (motion free) and **b** 3 h after (motion corrupted) KA injection. Each MTR_{asym} curve also shows the results before and after motion correction using the GradMC algorithm. (gray [**a**] and pink [**b**] dotted lines: without motion correction, and black [**a**] and red [**b**] solid lines: with motion correction).

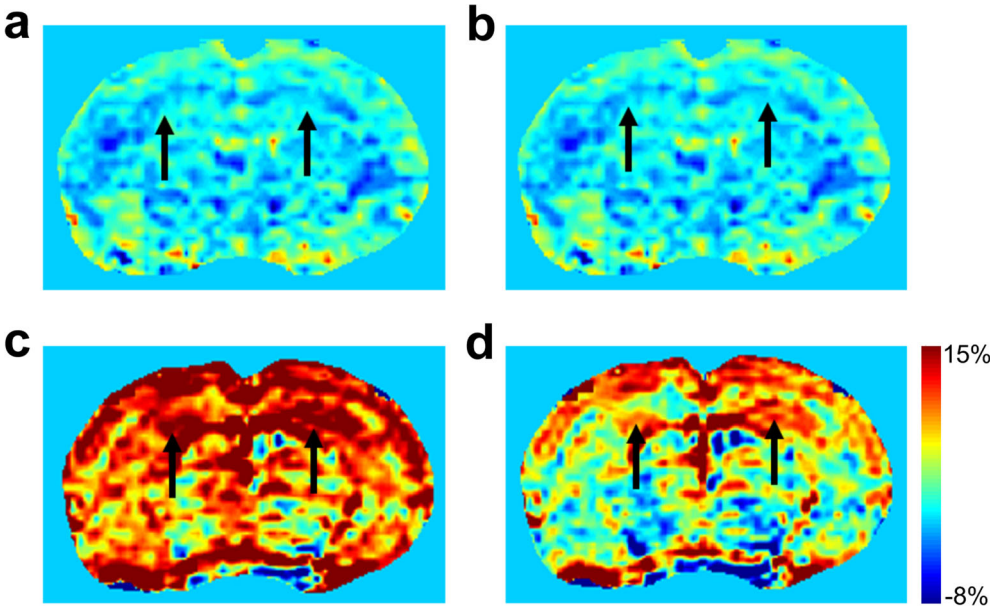

Fig. 4. Reconstructed GluCEST maps **a**, **c** without and **b**, **d** with motion correction using the GradMC algorithm before (motion free **a**, **b**) and after (motion corrupted, **c**, **d**) KA injection. Black arrows indicate the glutamate signal features in the hippocampus region.

motion correction, the whole brain appeared to have high glutamate concentrations, and signals in the hippocampus appeared to be over-estimated (black arrow; Fig. 4c) as compared with the result after motion correction (black arrow, Fig. 4d).

Discussion

To date, many successful approaches for motion correction have been introduced based on prospective and retrospective techniques [1, 4, 6, 7, 9, 23–26]. Prospective motion corrections can be involved in the use of information that is additionally acquired outside the receiver coil, with the help of motion tracking systems [6, 25, 26]. In a different way, retrospective motion corrections can be performed by constructing reference data by acquiring additional echoes through adjustment of the pulse sequence (navigator), without employing any external tracking systems [4, 7, 9]. These two approaches can ultimately yield motion-corrected results, but they may have limited applicability as they are costly and time-consuming, as additional systems or signals are needed. The GradMC explores possible motion space and selects a point in that space, such that the motion-corrected image yields the minimum value of the cost function [10, 11]. It iteratively corrects the translation and rotation from the initial information of the motion trajectory using the gradient entropy metric as a cost function. Interestingly, the GradMC can be easily applied to image motion correction by using only the acquired MR images, without the need for external motion tracking systems or specially modified pulse sequences.

In the current study, we applied the GradMC method to GluCEST data for evaluating the feasibility of motion correction in CEST imaging. Conventionally, in preclinical and clinical CEST imaging, subjects are constrained by administering anesthesia or by instructing them to remain motionless, which in effect causes motion to be nearly negligible. Therefore, the motion-correction procedure in CEST imaging generally uses an image registration method between the reference image (unsaturated image) and the images acquired at multiple offsets assuming no motion in the reference image. However, as seen in our experiments, it is difficult to perform motion correction using image registration during CEST image acquisition epileptic seizure, because even the reference image was already motion-corrupted. Therefore, instead of using an image registration method, we sought to apply another motion-correction method that can be used practically in CEST imaging in the context of a disorder involving involuntary motion, and selected the GradMC method for this study. Our results clearly showed that the GradMC could be used to correct for motion occurring during CEST imaging in a rat epileptic seizure model. In addition, our results showed negligible differences when applying the GradMC algorithm to motion-free data and found significant differences when applying it to motion-corrupted data, indicating that the GradMC algorithm effectively performed motion correction in this study, as we expected. Although there is no gold standard with which to compare our motion-correction results, in contrast to the numerous studies in which most motion correction algorithms have been applied, the efficacy of our approach can be sufficiently inferred from quantitative analysis and qualitative results from brain mapping images.

This study was designed to evaluate the effects of motion correction in GluCEST imaging. Since this study is limited to a pre-clinical epilepsy model using GluCEST imaging technique, further applications should be considered with various types of CEST imaging such as amide proton transfer, creatine CEST, glycogen CEST in the pre-clinical models, and human patients requiring motion correction to increase quantitative and qualitative accuracy. Moreover, the application of motion correction in this study was utilized single-slice CEST imaging on the hippocampus region. Moreover, future CEST image acquisitions with 2D or 3D multi-slices for applying motion correction and evaluating the level changes of exchangeable protons in detail would extend the results of the current study with the GradMC motion correction algorithm, which can be applied to 3D images as well as 2D images.

Conclusions

We applied a retrospective motion-correction method, named GradMC, which is capable of blind estimation and correction, to CEST imaging, to evaluate the feasibility of using motion correction in a rat model of epileptic seizure. The overall results clearly indicated that the GradMC could be a useful method for motion-correcting GluCEST images, yielding quantitatively and qualitatively improved results. The GradMC may greatly facilitate motion correction for various types of CEST imaging.

Funding Information This study was supported by grants from the Basic Science Research Program, through the National Research Foundation of Korea (NRF-2017R1A6A3A03012461, NRF-2018R1A2B2007694, and NRF-2018R1C1B6004521), and the Korea Health Technology R&D Project, through the Korea Health Industry Development Institute (HI14C1090), funded by the Ministry of Health and Welfare, Republic of Korea. This study was also supported by the 2017 University of Sydney Postdoctoral Fellowship Scheme (192237).

Compliance with Ethical Standards

Conflict of Interest

The authors declare that they have no conflict of interest.

References

1. Godenschweger F, Kagebein U, Stucht D et al (2016) Motion correction in MRI of the brain. Phys Med Biol 61:R32–R56
2. Wood ML, Henkelman RM (1985) MR image artifacts from periodic motion. Med Phys 12:143–151
3. Zaitsev M, Maclaren J, Herbst M (2015) Motion artifacts in MRI: a complex problem with many partial solutions. J Magn Reson Imaging 42:887–901
4. Kochunov P, Lancaster JL, Glahn DC, Purdy D, Laird AR, Gao F, Fox P (2006) Retrospective motion correction protocol for high-resolution anatomical MRI. Hum Brain Mapp 27:957–962
5. White N, Roddey C, Shankaranarayanan A, Han E, Rettmann D, Santos J, Kuperman J, Dale A (2010) PROMO: real-time prospective motion correction in MRI using image-based tracking. Magn Reson Med 63:91–105
6. Maclaren J, Herbst M, Speck O, Zaitsev M (2013) Prospective motion correction in brain imaging: a review. Magn Reson Med 69:621–636
7. Manduca A, McGee KP, Welch EB et al (2000) Autocorrection in MR imaging: adaptive motion correction without navigator echoes. Radiology 215:904–909
8. Lin W, Ladinsky GA, Wehrli FW, Song HK (2007) Image metric-based correction (autofocusing) of motion artifacts in high-resolution trabecular bone imaging. J Magn Reson Imaging 26:191–197
9. Lin W, Song HK (2006) Improved optimization strategies for autofocusing motion compensation in MRI via the analysis of image metric maps. Magn Reson Imaging 24:751–760
10. Loktyushin A, Nickisch H, Pohmann R, Scholkopf B (2013) Blind retrospective motion correction of MR images. Magn Reson Med 70:1608–1618
11. Loktyushin A, Nickisch H, Pohmann R, Schoelkopf B (2015) Blind multirigid retrospective motion correction of MR images. Magn Reson Med 73:1457–1468
12. Ward KM, Aletras AH, Balaban RS (2000) A new class of contrast agents for MRI based on proton chemical exchange dependent saturation transfer (CEST). J Magn Reson 143:79–87
13. Sherry AD, Woods M (2008) Chemical exchange saturation transfer contrast agents for magnetic resonance imaging. Annu Rev Biomed Eng 10:391–411
14. van Zijl PCM, Yadav NN (2011) Chemical exchange saturation transfer (CEST): what is in a name and what isn't? Magn Reson Med 65:927–948
15. Cai KJ, Haris M, Singh A, Kogan F, Greenberg JH, Hariharan H, Detre JA, Reddy R (2012) Magnetic resonance imaging of glutamate. Nat Med 18:302–306
16. Pepin J, Francelle L, Carrillo-de Sauvage MA et al (2016) In vivo imaging of brain glutamate defects in a knock-in mouse model of Huntington's disease. Neuroimage 139:53–64
17. Roalf DR, Nanga RPR, Rupert PE, Hariharan H, Quarmley M, Calkins ME, Dress E, Prabhakaran K, Elliott MA, Moberg PJ, Gur RC, Gur RE, Reddy R, Turetsky BI (2017) Glutamate imaging (GluCEST) reveals lower brain GluCEST contrast in patients on the psychosis spectrum. Mol Psychiatry 22:1298–1305
18. Davis KA, Nanga RPR, Das S, Chen SH, Hadar PN, Pollard JR, Lucas TH, Shinohara RT, Litt B, Hariharan H, Elliott MA, Detre JA, Reddy R (2015) Glutamate imaging (GluCEST) lateralizes epileptic foci in nonlesional temporal lobe epilepsy. Sci Transl Med 7(309):309ra161. https://doi.org/10.1126/scitranslmed.aaa7095
19. Hellier JL, Patrylo PR, Buckmaster PS, Dudek FE (1998) Recurrent spontaneous motor seizures after repeated low-dose systemic treatment with kainate: assessment of a rat model of temporal lobe epilepsy. Epilepsy Res 31:73–84
20. Lee DH, Lee DW, Kwon JI, Woo CW, Kim ST, Lee JS, Choi CG, Kim KW, Kim JK, Woo DC (2018) In vivo mapping and quantification of creatine using chemical exchange saturation transfer imaging in rat models of epileptic seizure. Mol Imaging Biol. https://doi.org/10.1007/s11307-018-1243-6
21. Eid T, Ghosh A, Wang Y, Beckstrom H, Zaveri HP, Lee TSW, Lai JCK, Malthankar-Phatak GH, de Lanerolle NC (2008) Recurrent seizures and brain pathology after inhibition of glutamine synthetase in the hippocampus in rats. Brain 131:2061–2070
22. Moreira JD, de Siqueira LV, Lague VM, Porciúncula LO, Vinadé L, Souza DO (2011) Short-term alterations in hippocampal glutamate transport system caused by one-single neonatal seizure episode: implications on behavioral performance in adulthood. Neurochem Int 59:217–223
23. Aksoy M, Forman C, Straka M, Çukur T, Hornegger J, Bammer R (2012) Hybrid prospective and retrospective head motion correction to mitigate cross-calibration errors. Magn Reson Med 67:1237–1251

24. Singh A, Cai KJ, Haris M, Hariharan H, Reddy R (2013) On B1 inhomogeneity correction of in vivo human brain glutamate chemical exchange saturation transfer contrast at 7T. Magn Reson Med 69:818–824
25. Zaitsev M, Dold C, Sakas G, Hennig J, Speck O (2006) Magnetic resonance imaging of freely moving objects: prospective real-time motion correction using an external optical motion tracking system. Neuroimage 31:1038–1050
26. Qin L, van Gelderen P, Derbyshire JA, Jin F, Lee J, de Zwart JA, Tao Y, Duyn JH (2009) Prospective head-movement correction for high-resolution MRI using an in-bore optical tracking system. Magn Reson Med 62:924–934